

## Average CsI Neutron Density Distribution from COHERENT Data

M. Cadeddu

Dipartimento di Fisica, Università degli Studi di Cagliari, and INFN, Sezione di Cagliari,  
Complesso Universitario di Monserrato—S.P. per Sestu Km 0.700, 09042 Monserrato (Cagliari), Italy

C. Giunti

INFN, Sezione di Torino, Via P. Giuria 1, I-10125 Torino, Italy

Y. F. Li<sup>\*</sup> and Y. Y. Zhang

Institute of High Energy Physics, Chinese Academy of Sciences, and School of Physical Sciences,  
University of Chinese Academy of Sciences, Beijing 100049, China



(Received 11 October 2017; revised manuscript received 21 December 2017; published 13 February 2018)

Using the coherent elastic neutrino-nucleus scattering data of the COHERENT experiment, we determine for the first time the average neutron rms radius of  $^{133}\text{Cs}$  and  $^{127}\text{I}$ . We obtain the practically model-independent value  $R_n = 5.5_{-1.1}^{+0.9}$  fm using the symmetrized Fermi and Helm form factors. We also point out that the COHERENT data show a  $2.3\sigma$  evidence of the nuclear structure suppression of the full coherence.

DOI: 10.1103/PhysRevLett.120.072501

The COHERENT experiment [1] observed for the first time coherent elastic neutrino-nucleus scattering with a small scintillator detector made of sodium-doped CsI exposed to a low-energy neutrino flux generated in the Spallation Neutron Source at Oak Ridge National Laboratory. Coherent elastic neutrino-nucleus scattering can occur if  $qR \ll 1$ , where  $q = |\vec{q}|$  is the three-momentum transfer and  $R$  is the nuclear radius [2,3].

The coherent elastic scattering of a neutrino with a nucleus can be observed by measuring very low values of the nuclear kinetic recoil energy  $T$ . For  $T \ll E$ , where  $E$  is the neutrino energy, we have  $q^2 \simeq 2MT$ , where  $M$  is the nuclear mass, and  $T_{\max} \simeq 2E^2/M$  [4]. For a nucleus with mass  $M \approx 100$  GeV and radius  $R \approx 5$  fm, elastic neutrino-nucleus scattering is coherent for  $T \ll (2MR^2)^{-1} \approx 10$  keV and it is required to have a neutrino beam with energy of the order of  $\sqrt{MT/2} \approx 20$  MeV.

The differential cross section for coherent elastic scattering of a neutrino with a nucleus  $\mathcal{N}$  with  $Z$  protons and  $N$  neutrons is given by [4–7]

$$\frac{d\sigma_{\nu-\mathcal{N}}}{dT}(E, T) \simeq \frac{G_F^2 M}{4\pi} \left(1 - \frac{MT}{2E^2}\right) [NF_N(q^2) - \epsilon ZF_Z(q^2)]^2, \quad (1)$$

where  $G_F$  is the Fermi constant,  $M$  is the nuclear mass,  $F_N(q^2)$  and  $F_Z(q^2)$  are, respectively, the nuclear neutron and proton form factors, and  $\epsilon = 1 - 4 \sin^2 \vartheta_W = 0.0454 \pm 0.0003$ , using the low-energy PDG value of the weak mixing angle  $\vartheta_W$  [8]. Because of the small value of  $\epsilon$ , the neutron contribution is dominant. Hence, measurements of the process give information on the nuclear neutron form factor, which is more difficult to obtain than the information on the proton nuclear form factor, that can be obtained with elastic electron-nucleus scattering and other electromagnetic processes (see Refs. [9,10]). Knowledge of these form factors is important, because form factors are the Fourier transform of the corresponding charge distribution. Electromagnetic processes probe the nuclear proton distribution, whereas neutral-current weak interaction processes are mainly sensitive to the nuclear neutron distribution. Also hadron scattering experiments give information on the nuclear neutron distribution, but their interpretation depends on the model used to describe nonperturbative strong interactions (see Refs. [11–14]). Before the COHERENT experiment, the only measurement of the nuclear neutron distribution with neutral-current weak interactions was done with parity-violating electron scattering on  $^{208}\text{Pb}$  in the PREX experiment [15].

The measurement of the nuclear neutron density distribution is a topic of broad interest in the physics community. In particular, the corresponding rms radius  $R_n$  and the difference between  $R_n$  and the rms radius  $R_p$  of the proton distribution (the so-called “neutron skin”) are crucial ingredients of the nuclear matter equation of state (EOS), which plays an essential role in understanding

Published by the American Physical Society under the terms of the Creative Commons Attribution 4.0 International license. Further distribution of this work must maintain attribution to the author(s) and the published article's title, journal citation, and DOI. Funded by SCOAP<sup>3</sup>.

several processes, like nuclei in laboratory experiments, heavy ion collisions, and the structure and evolution of compact astrophysical objects as neutron stars (see Refs. [16–20]).

In the case of the COHERENT experiment, the coherent elastic scattering is measured on  $^{133}\text{Cs}$  and  $^{127}\text{I}$ , which contribute incoherently, leading to the total cross section

$$\frac{d\sigma_{\nu-\text{CsI}}}{dT} = \frac{d\sigma_{\nu-\text{Cs}}}{dT} + \frac{d\sigma_{\nu-\text{I}}}{dT}, \quad (2)$$

with  $N_{\text{Cs}} = 78$ ,  $Z_{\text{Cs}} = 55$ ,  $N_{\text{I}} = 74$ , and  $Z_{\text{I}} = 53$ . We neglect the small axial contribution due to the unpaired valence proton [5].

The proton and neutron form factors are the Fourier transform of the nuclear proton and neutron densities. The proton structures of  $^{133}\text{Cs}$  and  $^{127}\text{I}$  have been studied with muonic atom spectroscopy [9] and the data were fitted with Fermi density distributions of the form

$$\rho_F(r) = \frac{\rho_0}{1 + e^{(r-c)/a}}, \quad (3)$$

where  $\rho_0$  is a normalization factor and  $a$  is a parameter which quantifies the surface thickness  $t = 4a \ln 3$ , which was fixed at 2.30 fm. The fit of the data yielded  $c_{\text{Cs}} = 5.6710 \pm 0.0001$  and  $c_{\text{I}} = 5.5931 \pm 0.0001$  fm, which correspond to the proton rms radii

$$R_p^{\text{Cs}} = \langle r_p^2 \rangle_{\text{Cs}}^{1/2} = 4.804 \text{ fm}, \quad (4)$$

$$R_p^{\text{I}} = \langle r_p^2 \rangle_{\text{I}}^{1/2} = 4.749 \text{ fm}. \quad (5)$$

Hence, the proton structures of  $^{133}\text{Cs}$  and  $^{127}\text{I}$  are similar. Since we expect that also their neutron structures are similar and the current uncertainties of the COHERENT data do not allow us to distinguish between them, we consider in Eq. (2) the approximation

$$F_{N,\text{Cs}}(q^2) \simeq F_{N,\text{I}}(q^2) \simeq F_N(q^2). \quad (6)$$

We fitted the COHERENT data under this approximation assuming proton form factors  $F_Z(q^2)$  for  $^{133}\text{Cs}$  and  $^{127}\text{I}$  given by the Fourier transform of a symmetrized Fermi (SF) distribution  $\rho_{\text{SF}}(r) = \rho_F(r) + \rho_F(-r) - 1$ , which is practically equivalent to a Fermi distribution and gives an analytic expression for the form factor [21]:

$$F_Z^{\text{SF}}(q^2) = \frac{3}{qc[(qc)^2 + (\pi qa)^2]} \left( \frac{\pi qa}{\sinh(\pi qa)} \right) \times \left( \frac{\pi qa \sin(qc)}{\tanh(\pi qa)} - qc \cos(qc) \right). \quad (7)$$

In order to get information on the neutron distribution of  $^{133}\text{Cs}$  and  $^{127}\text{I}$  in the approximation in Eq. (6), we

considered the following parametrizations of the neutron form factor  $F_N(q^2)$ : (1) A symmetrized Fermi form factor  $F_N^{\text{SF}}(q^2)$  analogous to that in Eq. (7). In this case, the neutron rms radius is given by

$$R_n^2 = \frac{3}{5} c^2 + \frac{7}{5} (\pi a)^2. \quad (8)$$

Since the COHERENT data are not sensitive to the surface thickness, we consider the same value of  $t = 2.30$  fm as for the proton form factor. We verified that the results of the fit are practically independent of small variations of the value of the surface thickness. (2) The Helm form factor [22]

$$F_N^{\text{Helm}}(q^2) = 3 \frac{j_1(qR_0)}{qR_0} e^{-q^2 s^2/2}, \quad (9)$$

where  $j_1(x) = \sin(x)/x^2 - \cos(x)/x$  is the spherical Bessel function of order one and  $R_0$  is the box (or diffraction) radius. In this case, the neutron rms radius is given by

$$R_n^2 = \frac{3}{5} R_0^2 + 3s^2. \quad (10)$$

The parameter  $s$  quantifies the surface thickness. In this case we consider the value  $s = 0.9$  fm which was determined for the proton form factor of similar nuclei [23]. Also in this case, we verified that the results of the fit are practically independent of small variations of the value of the surface thickness.

We fitted the COHERENT data in Fig. 3A of Ref. [1] with the least-squares function

$$\chi^2 = \sum_{i=4}^{15} \left( \frac{N_i^{\text{exp}} - (1 + \alpha)N_i^{\text{th}} - (1 + \beta)B_i}{\sigma_i} \right)^2 + \left( \frac{\alpha}{\sigma_\alpha} \right)^2 + \left( \frac{\beta}{\sigma_\beta} \right)^2. \quad (11)$$

For each energy bin  $i$ ,  $N_i^{\text{exp}}$  and  $N_i^{\text{th}}$  are, respectively, the experimental and theoretical number of events,  $B_i$  is the estimated number of background events extracted from Fig. S13 of Ref. [1], and  $\sigma_i$  is the statistical uncertainty.  $\alpha$  and  $\beta$  are nuisance parameters which quantify, respectively, the systematic uncertainty of the signal rate and the systematic uncertainty of the background rate. The corresponding standard deviations are  $\sigma_\alpha = 0.28$  and  $\sigma_\beta = 0.25$  [1]. We did not consider the first three energy bins in Fig. 3A of Ref. [1], which do not give any information on neutrino-nucleus scattering because they correspond to the detection of less than 6 photoelectrons, for which the acceptance function in Fig. S9 of Ref. [1] vanishes. We considered only the 12 energy bins from  $i = 4$  to  $i = 15$  for which the COHERENT Collaboration fitted the quenching factor in Fig. S10 of Ref. [1] and obtained the linear relation

between the observed number of photoelectrons  $N_{\text{PE}}$  and the nuclear kinetic recoil energy  $T$  given by

$$N_{\text{PE}} = 1.17 \left( \frac{T}{\text{keV}} \right). \quad (12)$$

The theoretical number of coherent elastic scattering events  $N_i^{\text{th}}$  in each energy bin  $i$  depends on the nuclear neutron form factor and it is given by

$$N_i^{\text{th}} = N_{\text{CsI}} \int_{T_i}^{T_{i+1}} dT \int_{E_{\min}} dEA(T) \frac{dN_{\nu}}{dE} \frac{d\sigma_{\nu-\text{CsI}}}{dT}, \quad (13)$$

where  $N_{\text{CsI}}$  is the number of CsI in the detector (given by  $N_A M_{\text{det}} / M_{\text{CsI}}$ , where  $N_A$  is the Avogadro number,  $M_{\text{det}} = 14.6$  kg, is the detector mass, and  $M_{\text{CsI}} = 259.8$  is the molar mass of CsI),  $E_{\min} = \sqrt{MT/2}$ ,  $A(T)$  is the acceptance function given in Fig. S9 of Ref. [1] and  $dN_{\nu}/dE$  is the neutrino flux integrated over the experiment lifetime. Neutrinos at the Spallation Neutron Source consist of a prompt component of monochromatic  $\nu_{\mu}$  from stopped pion decays,  $\pi^+ \rightarrow \mu^+ + \nu_{\mu}$ , and two delayed components of  $\bar{\nu}_{\mu}$  and  $\nu_e$  from the subsequent muon decays,  $\mu^+ \rightarrow e^+ + \bar{\nu}_{\mu} + \nu_e$ . The total flux  $dN_{\nu}/dE$  is the sum of

$$\frac{dN_{\nu_{\mu}}}{dE} = \eta \delta \left( E - \frac{m_{\pi}^2 - m_{\mu}^2}{2m_{\pi}} \right), \quad (14)$$

$$\frac{dN_{\nu_{\bar{\mu}}}}{dE} = \eta \frac{64E^2}{m_{\mu}^3} \left( \frac{3}{4} - \frac{E}{m_{\mu}} \right), \quad (15)$$

$$\frac{dN_{\nu_e}}{dE} = \eta \frac{192E^2}{m_{\mu}^3} \left( \frac{1}{2} - \frac{E}{m_{\mu}} \right), \quad (16)$$

for  $E \leq m_{\mu}/2 \simeq 52.8$  MeV, with the normalization factor  $\eta = rN_{\text{POT}}/4\pi L^2$ , where  $r = 0.08$  is the number of neutrinos per flavor that are produced for each proton on target,  $N_{\text{POT}} = 1.76 \times 10^{23}$  is the number of proton on target and  $L = 19.3$  m is the distance between the source and the COHERENT CsI detector [1].

Figure 1 shows the COHERENT data as a function of the nuclear kinetic recoil energy  $T$ . We first compared the data with the predictions in the case of full coherence, i.e., all nuclear form factors equal to unity. Figure 1 shows that the corresponding histogram does not fit the data. Hence, albeit the COHERENT data represent the first measurement of coherent elastic neutrino-nucleus scattering, the scattering is not fully coherent and the data give information on the nuclear structure. Indeed, the COHERENT Collaboration [1] explained the data using the form factor in Ref. [24] with fixed value of the parameters, i.e., assuming the value of the nuclear rms radius.

We fitted the COHERENT data in order to get information on the value of the neutron rms radius  $R_n$ , which is determined by the minimization of the  $\chi^2$  in Eq. (11) using the symmetrized Fermi and Helm form factors. In both cases we obtained a minimum  $\chi^2$ , which is smaller than the  $\chi^2$  corresponding to full coherence by 5.5. Hence, the hypothesis of full coherence has a  $p$ -value of 1.9% and there is a  $2.3\sigma$  evidence of the nuclear structure suppression of the coherence.

Figure 1 shows the best-fit results that we obtained using the symmetrized Fermi and Helm form factors. Figure 2 shows the corresponding marginal values of the  $\chi^2$  as a function of  $R_n$ . One can see from both figures that the two parametrizations of the neutron form factor fit equally well the data and give practically the same result:

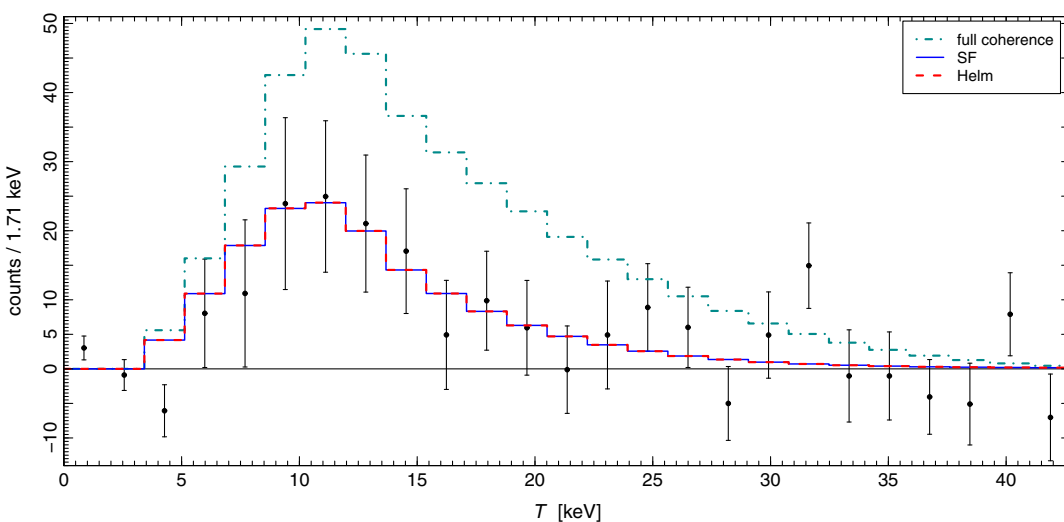


FIG. 1. COHERENT data [1] versus the nuclear kinetic recoil energy  $T$ . The histograms represent the theoretical prediction in the case of full coherence (cyan dash-dotted line) and the best fits obtained using the symmetrized Fermi distribution (blue solid line) and Helm (red dashed line) form factors.

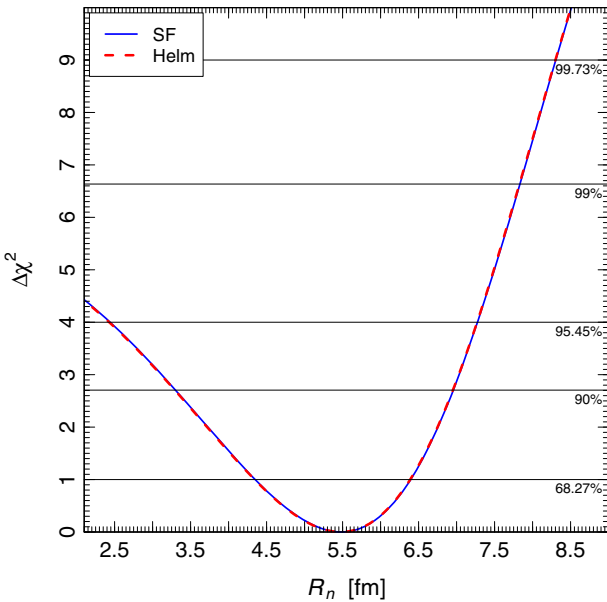


FIG. 2.  $\Delta\chi^2 = \chi^2 - \chi^2_{\min}$  as a function of the neutron rms radius  $R_n$  obtained from the fit of the data of the COHERENT experiment [1] using the symmetrized Fermi and Helm form factors.

$$R_n = 5.5^{+0.9}_{-1.1} \text{ fm.} \quad (17)$$

This is the first determination of the neutron rms radius of a nucleus obtained with neutrino-nucleus scattering data. Note also that it is practically model independent, because it coincides for the symmetrized Fermi and Helm form factors which correspond to reasonable descriptions of the nuclear density.

As already stated, the neutron rms radius was determined before only for  $^{208}\text{Pb}$  from the parity-violating measurements of the PREX experiment [15]. The authors of Ref. [25] found  $R_n(^{208}\text{Pb}) = 5.75 \pm 0.18$  fm. Our best-fit value of  $R_n$  for  $^{127}\text{I}$  and  $^{133}\text{Cs}$ , obtained assuming that the two nuclei have similar structures, is correctly smaller than that of the heavier  $^{208}\text{Pb}$  nucleus.

Table I shows the theoretical values of the proton and neutron rms radii of  $^{133}\text{Cs}$  and  $^{127}\text{I}$  obtained with nuclear

mean field models. All the models predict values of  $R_p$ , which are in approximate agreement with the experimental ones in Eqs. (4) and (5). Because of the large uncertainty, the average CsI value of  $R_n$  that we obtained in Eq. (17) is compatible with all the model calculations. It tends to favor values of  $R_n$  that are larger than all the model calculations in Table I, but more precise measurements are needed in order to truly test the models.

Another quantity of interest is the difference between the neutron and proton rms radii  $\Delta R_{np} = R_n - R_p$ , which is usually referred to as “neutron skin” [34]. The values of  $R_p$  for  $^{127}\text{I}$  and  $^{133}\text{Cs}$  determined in Ref. [9] are around 4.78 fm, with a difference of about 0.05 fm. Hence, for the neutron skin, we obtain

$$\Delta R_{np} \simeq 0.7^{+0.9}_{-1.1} \text{ fm.} \quad (18)$$

Unfortunately, the uncertainty is large and it does not allow us to claim a determination of the neutron skin. We can only note that the best-fit value indicates the possibility of a value that is larger than the model-predicted values in Table I, which are between about 0.1 and 0.2 fm (see also Ref. [34]).

Future data of the COHERENT experiment may lead to a better determination of the neutron rms radius  $R_n$  and of the neutron skin  $\Delta R_{np}$ . Figure 3 shows our estimation of the sensitivity to  $R_n$  of the COHERENT experiment as a function of the number of protons on target with the current systematic uncertainties, with half the current systematic uncertainties, and with one-quarter of the current systematic uncertainties. We have included the effect of the beam-off background, which we extracted from the statistical uncertainties of Fig. 3A of Ref. [1]. From Fig. 3 one can see that the current sensitivity gives a relative uncertainty  $\Delta R_n/R_n \simeq 17\%$ , which is in approximate agreement with the uncertainty of the determination of  $R_n$  in Eq. (17). With the current systematic uncertainties and 10 times the current number of protons on target, the data of the COHERENT experiment will allow us to determine  $R_n$  within about 0.5 fm. If the systematic uncertainties are

TABLE I. Theoretical values in units of fermi of the proton and neutron rms radii of  $^{133}\text{Cs}$  and  $^{127}\text{I}$  and the CsI average obtained with nonrelativistic Skyrme-Hartree-Fock (SHF) and relativistic mean field (RMF) nuclear models.

Model	$^{133}\text{Cs}$			$^{127}\text{I}$			CsI		
	$R_p$	$R_n$	$R_n - R_p$	$R_p$	$R_n$	$R_n - R_p$	$R_p$	$R_n$	$R_n - R_p$
SHF SkM* [26]	4.76	4.90	0.13	4.71	4.84	0.13	4.73	4.86	0.13
SHF SkP [27]	4.79	4.91	0.12	4.72	4.84	0.12	4.75	4.87	0.12
SHF SkI4 [28]	4.73	4.88	0.15	4.67	4.81	0.14	4.70	4.83	0.14
SHF Sly4 [29]	4.78	4.90	0.13	4.71	4.84	0.13	4.73	4.87	0.13
SHF UNEDF1 [30]	4.76	4.90	0.15	4.68	4.83	0.15	4.71	4.87	0.15
RMF NL-SH [31]	4.74	4.93	0.19	4.68	4.86	0.19	4.71	4.89	0.18
RMF NL3 [32]	4.75	4.95	0.21	4.69	4.89	0.20	4.72	4.92	0.20
RMF NL-Z2 [33]	4.79	5.01	0.22	4.73	4.94	0.21	4.76	4.97	0.21

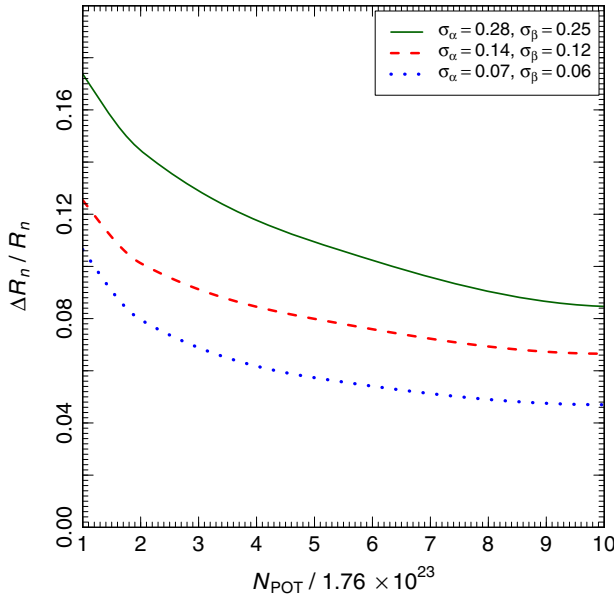


FIG. 3. Projected relative uncertainty of the possible determination of the neutron rms radius  $R_n$  with the data of the COHERENT experiment as a function of the number  $N_{\text{POT}}$  of protons on target in units of the current number ( $1.76 \times 10^{23}$ ) for the current systematic uncertainties (solid green curve), half the current systematic uncertainties (dashed red curve), and one-quarter of the current systematic uncertainties (dotted blue curve).

reduced by half or one-quarter,  $R_n$  can be determined within about 0.4 or 0.3 fm, respectively. Such a measurement would also decrease the uncertainty on the value of the neutron skin, allowing a more meaningful comparison with the model predictions in Table I.

Since  $R_p$  is relatively well known, a measurement of  $R_n$  allows us to determine the neutron skin  $\Delta R_{np}$ . Information on this quantity is eagerly awaited because  $\Delta R_{np}$  is correlated with several properties characterizing neutron-rich matter (see Refs. [16–20]). A larger neutron skin would suggest a stiffer EOS and imply a larger neutron star radius  $R_{\text{NS}}$ . Since the neutron star binding energy is inversely proportional to  $R_{\text{NS}}$ , a larger  $R_{\text{NS}}$  implies a smaller gravitational binding energy, which can be tested by observing the intense neutrino burst of a core collapse supernova.

The neutron skin is also correlated with several other nuclear quantities, e.g., with the slope of bulk symmetry energy, with the slope of binding energy of neutron matter, and with the symmetry correction to the incompressibility (see Ref. [35] for a review).

On August 17, 2017 the Advanced LIGO and Advanced Virgo gravitational-wave detectors made their first observation of a binary neutron star inspiral [36]. From this observation the Collaboration was able to infer not only the component masses of the binary but also the tidal deformability parameter, which is related to the neutron star EOS and to the neutron skin [37,38].

Information on the nuclear neutron density radius  $R_n$  is also important for a precise determination of the background due to coherent elastic neutrino-nucleus scattering in dark matter detectors. This background will crucially limit the discovery potential of future dark matter detectors [39]. Until now, the background has been evaluated using a unique Helm nuclear form factor for protons and neutrons, with the Lewin-Smith prescription [40] for the input value of the nuclear radii. Since cesium and iodine have similar atomic and mass numbers to that of xenon, it is possible to make an estimation of the impact of the inclusion of different proton and neutron form factors (with the value of  $R_n$  found in this paper) on the neutrino background for experiments like DARWIN [41], XENONnT [42], and LZ [43], that use xenon as a target.

In conclusion, we have determined for the first time the neutron rms radius of  $^{133}\text{Cs}$  and  $^{127}\text{I}$  (assuming that they have similar structures) from the fit of the data on coherent elastic neutrino-nucleus scattering of the COHERENT experiment. Considering the symmetrized Fermi and Helm form factors, we obtained the practically model-independent value  $R_n = 5.5_{-1.1}^{+0.9}$  fm. We also found that the COHERENT data show a  $2.3\sigma$  evidence of the nuclear structure suppression of the full coherence.

M. C. wishes to thank M. Lissia for useful discussions. C. G. is grateful to S. M. Bilenky and M. V. Garzelli for stimulating discussions. The work of Y. F. L. and Y. Y. Z. was supported in part by the National Natural Science Foundation of China under Grant No. 11305193 and by the Strategic Priority Research Program of the Chinese Academy of Sciences under Grant No. XDA10010100. Y. F. L. is also grateful for the support by the CAS Center for Excellence in Particle Physics (CCEPP).

\*Corresponding author.

liyufeng@ihep.ac.cn

- [1] D. Akimov *et al.* (COHERENT Collaboration), *Science* **357**, 1123 (2017).
- [2] D. Z. Freedman, *Phys. Rev. D* **9**, 1389 (1974).
- [3] D. Z. Freedman, D. N. Schramm, and D. L. Tubbs, *Ann. Rev. Nucl. Part. Sci.* **27**, 167 (1977).
- [4] A. Drukier and L. Stodolsky, *Phys. Rev. D* **30**, 2295 (1984).
- [5] J. Barranco, O. G. Miranda, and T. I. Rashba, *J. High Energy Phys.* **12** (2005) 021.
- [6] K. Patton, J. Engel, G. C. McLaughlin, and N. Schunck, *Phys. Rev. C* **86**, 024612 (2012).
- [7] D. K. Papoulias and T. S. Kosmas, *Adv. High Energy Phys.* **2015** 763648 (2015).
- [8] C. Patrignani *et al.* (Particle Data Group), *Chin. Phys. C* **40**, 100001 (2016).
- [9] G. Fricke, C. Bernhardt, K. Heilig, L. A. Schaller, L. Schellenberg, E. B. Shera, and C. W. de Jager, *At. Data Nucl. Data Tables* **60**, 177 (1995).
- [10] I. Angeli and K. P. Marinova, *At. Data Nucl. Data Tables* **99**, 69 (2013).

- [11] C. Garcia-Recio, J. Nieves, and E. Oset, *Nucl. Phys.* **A547**, 473 (1992).
- [12] V. E. Starodubsky and N. M. Hintz, *Phys. Rev. C* **49**, 2118 (1994).
- [13] A. Trzcinska, J. Jastrzebski, P. Lubinski, F. J. Hartmann, R. Schmidt, T. von Egidy, and B. Klos, *Phys. Rev. Lett.* **87**, 082501 (2001).
- [14] B. C. Clark, L. J. Kerr, and S. Hama, *Phys. Rev. C* **67**, 054605 (2003).
- [15] S. Abrahanyan *et al.* (PREX Collaboration), *Phys. Rev. Lett.* **108**, 112502 (2012).
- [16] B. A. Brown, *Phys. Rev. Lett.* **85**, 5296 (2000).
- [17] C. J. Horowitz and J. Piekarewicz, *Phys. Rev. Lett.* **86**, 5647 (2001).
- [18] P. G. Reinhard and W. Nazarewicz, *Phys. Rev. C* **81**, 051303 (2010).
- [19] M. B. Tsang *et al.*, *Phys. Rev. C* **86**, 015803 (2012).
- [20] G. Hagen *et al.*, *Nat. Phys.* **12**, 186 (2016).
- [21] J. Piekarewicz, A. R. Linero, P. Giuliani, and E. Chicken, *Phys. Rev. C* **94**, 034316 (2016).
- [22] R. H. Helm, *Phys. Rev.* **104**, 1466 (1956).
- [23] J. Friedrich and N. Voegler, *Nucl. Phys.* **A373**, 192 (1982).
- [24] S. R. Klein and J. Nystrand, *Phys. Rev. C* **60**, 014903 (1999).
- [25] C. J. Horowitz *et al.*, *Phys. Rev. C* **85**, 032501 (2012).
- [26] J. Bartel, P. Quentin, M. Brack, C. Guet, and H. B. Hakansson, *Nucl. Phys.* **A386**, 79 (1982).
- [27] J. Dobaczewski, H. Flocard, and J. Treiner, *Nucl. Phys.* **A422**, 103 (1984).
- [28] P. G. Reinhard and H. Flocard, *Nucl. Phys.* **A584**, 467 (1995).
- [29] E. Chabanat, P. Bonche, P. Haensel, J. Meyer, and R. Schaeffer, *Nucl. Phys.* **A635**, 231 (1998).
- [30] M. Kortelainen, J. McDonnell, W. Nazarewicz, P. G. Reinhard, J. Sarich, N. Schunck, M. V. Stoitsov, and S. M. Wild, *Phys. Rev. C* **85**, 024304 (2012).
- [31] M. M. Sharma, M. A. Nagarajan, and P. Ring, *Phys. Lett. B* **312**, 377 (1993).
- [32] G. A. Lalazissis, J. Konig, and P. Ring, *Phys. Rev. C* **55**, 540 (1997).
- [33] M. Bender, K. Rutz, P. G. Reinhard, J. A. Maruhn, and W. Greiner, *Phys. Rev. C* **60**, 034304 (1999).
- [34] C. J. Horowitz, S. J. Pollock, P. A. Souder, and R. Michaels, *Phys. Rev. C* **63**, 025501 (2001).
- [35] M. Baldo and G. F. Burgio, *Prog. Part. Nucl. Phys.* **91**, 203 (2016).
- [36] B. P. Abbott *et al.* (Virgo, LIGO Scientific Collaborations), *Phys. Rev. Lett.* **119**, 161101 (2017).
- [37] B. Kumar, B. K. Agrawal, and S. K. Patra, arXiv:1711.04940.
- [38] F. J. Fattoyev, J. Piekarewicz, and C. J. Horowitz, arXiv: 1711.06615.
- [39] J. Billard, E. Figueroa-Feliciano, and L. Strigari, *Phys. Rev. D* **89**, 023524 (2014).
- [40] J. D. Lewin and P. F. Smith, *Astropart. Phys.* **6**, 87 (1996).
- [41] J. Aalbers *et al.*, *J. Cosmol. Astropart. Phys.* **11** (2016) 017.
- [42] E. Aprile *et al.* (XENON Collaboration), *J. Cosmol. Astropart. Phys.* **04** (2016) 027.
- [43] B. J. Mount *et al.*, arXiv:1703.09144.